# Dissociative electron attachment and vibrational excitation of $H_2$ by low-energy electrons: Calculations based on an improved nonlocal resonance model

J. Horáček,* M. Čížek, K. Houfek, and P. Kolorenč
*Institute of Theoretical Physics, Charles University, Prague, Czech Republic*

W. Domcke
*Department of Chemistry, Technical University of Munich, D-85747 Garching, Germany*
(Received 21 May 2004; published 23 November 2004)

An improved nonlocal resonance model proposed by Čížek, Horáček, and Domcke [J. Phys. B **31**, 2571 (1998)] is used for the calculation of cross sections of electron dissociative attachment and vibrational excitation of molecular hydrogen by the impact of low-energy electrons in the range of $^2\Sigma_u^+$ resonance. The model is based on *ab initio* data and takes full account of the nonlocality of the effective potential for the nuclear motion. The dissociative attachment cross sections and rate constants are calculated for all target states $(v,J)$ of relevance and compared with other theoretical and experimental data. It is found that the present dissociative attachment cross section calculated under the conditions of the experiment carried out by Schulz and Asundi reproduces the larger of the two values proposed by them, i.e.–$2.8\times10^{-21}$ cm$^2$. A detailed discussion of the dissociative attachment cross section as a function of the vibrational and rotational target states is given. Very narrow peaks, with a width of 1 meV, are observed in the dissociative attachment cross section for large values of the orbital quantum number $J$. These structures are interpreted as shape resonances in $H^-+H$ collision dynamics. It is shown that for large values of $J$ rotational excitation of the hydrogen molecule enhances the dissociative attachment more efficiently than vibrational excitation. The largest dissociative attachment cross section of $28.3\times10^{-16}$ cm$^2$ is obtained for $v=1$ and $J=29$. The process of vibrational excitation will be discussed in a separate paper.

DOI: 10.1103/PhysRevA.70.052712 PACS number(s): 34.80.Ht

## I. INTRODUCTION

The processes of dissociative electron attachment (DA)

$$e + H_2(v_i,J_i) \rightarrow H + H^-, \tag{1}$$

associative detachment (AD)

$$H + H^- \rightarrow e + H_2(v_f,J_f), \tag{2}$$

and vibrational excitation (VE)

$$e + H_2(v_i,J_i) \rightarrow e + H_2(v_f,J_i) \tag{3}$$

play a decisive role in many applications. In astrophysics, for example, it is assumed [1] that the process of AD is responsible for the creation of the hydrogen molecule in early stages of the development of the Universe. The existence of molecular hydrogen represents a very efficient cooling mechanism of hot matter which eventually leads to the creation of stars, galaxies, etc. It was suggested [2,3] that DA to vibrationally excited molecular hydrogen plays an important role in molecular-activated recombination in fusion divertor plasmas. This process is also believed to be the primary source of negative-ion production in low-density hydrogen plasmas; see, e.g., [4–6].

In addition, these processes are of importance in gas lasers, planetary atmospheres, etc. The inelastic electron scattering from $H_2$ may also have some significance for the understanding of molecular conductance [7].

The production of $H^-$ in the process $e+H_2\rightarrow H+H^-$ was first observed by Kchvostenko and Dukelskij almost 50 years ago [8] and studied later in detail by Schulz [9] and Schulz and Asundi [10]. It was found that the DA cross section peaks at 3.75 eV with a magnitude of about $10^{-5}$ Å$^2$; two higher peaks are observed at energies of 8 eV and 14 eV. The magnitude of the low-energy peak is measured relative to the strong 14-eV peak, for which two values were reported [10]. Consequently, two values of the magnitude of the low-energy DA cross section are found in the literature [10]: $1.6\times10^{-5}$ Å$^2$ (this generally accepted value is based on Rapp's measurement [11] of the 14-eV peak) and $2.8\times10^{-5}$ Å$^2$, based on the measurement of Schulz [9]. An extraordinarily strong isotope effect was observed in this energy range by Rapp *et al.* [11] and Schulz and Asundi [12]. The shape of the DA cross section was remeasured recently by Drexel *et al.* [13]. The DA cross section at higher temperatures, $T=1400$ K for $H_2$ and 1350 K for $D_2$, was measured by Allan and Wong [14]. The DA cross section was found to increase very rapidly with increasing temperature, indicating a strong dependence of the DA on the vibrational quantum number of the target.

A large effort has been devoted to the development of a theoretical description of the DA, AD, and VE processes, ranging from simple phenomenological models to elaborate models involving all essential ingredients of the processes, in particular also the nonlocality of the effective nuclear potential stemming from the breakdown of the Born-Oppenheimer approximation during the energy transfer from the electronic degrees of freedom to the nuclear motion. A vast literature is

*Electronic address: horacek@mbox.troja.mff.cuni.cz

 

devoted to the theoretical study of the DA process in molecular hydrogen (see [15] for a recent review). Although there were some attempts to describe the process directly using the zero-range potential approximation [16] or the frame-transformation method [17], most of the calculations were based on the assumption that a metastable anion state (shape resonance) is formed during the collision. The initial studies employed the local-complex-potential approximation [18–23]. The data of local-complex-potential calculations with a semiempirical potential [19,22] are used for plasma modeling [24] up to date. In the work of Domcke and collaborators [25,26] the vibrational dynamics of $H_2^-$ was treated using the nonlocal energy dependent effective potential, resulting from the use of the Feshbach projection operator formalism, without any further approximations. The time-dependent version of the theory was also derived and used to calculate DA cross sections for $H_2$ [27,28]. It was found that the cross section for DA to the ground state of the hydrogen molecule differs from the one obtained within the local complex potential approximation by one order of magnitude. Since it is time consuming to treat the dynamics using the full nonlocal potential for many rovibrational states of the target molecule, some approximations halfway between the nonlocal resonance description and the local complex potential approximation have been derived [29–31]. The semiclassical version of the nonlocal resonance theory has also been derived by Fabrikant and co-workers and applied to calculate DA to a rovibrationally excited $H_2$ molecule [15,32–36]. Efficient numerical methods which account fully for the nonlocal effects for arbitrary rovibrational states of diatomic molecules were developed and implemented by the present authors, [37–39].

It is the purpose of this paper to present the results of calculations of a complete set of cross sections of DA and VE processes based on the use of the improved nonlocal resonance model (NRM) of Čížek, Horáček, and Domcke [39]. This models differs from previous *ab initio*—based nonlocal resonance models [25,27] by a more accurate description of the long-range part of the $H_2^-$ potential-energy function [40]. The paper [39] was focused on the AD process, which has not been studied with a nonlocal resonance model before. Since the model represents (to our knowledge) the most accurate treatment of the dynamics of the vibrational motion of the $H_2^-$ collision complex, we found it useful to present and discuss a complete set of data for inelastic low-energy electron $H_2$ scattering within this model.

The present work is published in two parts. The process of DA is discussed in the first part, while vibrational excitation is studied in the second part. We will refer to these parts as papers I and II in the following. Paper I is organized as follows. The basic theory and the numerical methods used are briefly explained in Sec. II. Section III contains the main results of the present work. The role of target excitation (rotational and vibrational) on the DA cross section is discussed. The calculated cross sections are compared with the experimental data of Schultz and Asundi [10] and Drexel *et al.* [13]. The temperature effect on DA is also discussed and the calculated cross sections are compared with the experimental data of Allan and Wong [14]. Finally, the present DA cross sections are compared with the results of several other calculations. It is found that there are significant discrepancies among the various theories as far as the ground-state DA cross section is concerned. In Sec. IV, narrow resonances found in the DA cross sections of highly rotationally excited $H_2$ are discussed. Section V is devoted to the study of isotope effects. The results are summarized in Sec. VI. The model used for the calculations is described in detail in the Appendix. The process of vibrational excitation of hydrogen by electron impact will be addressed in a separate paper.

## II. BASIC THEORY

### A. Description of the DA process

The nonlocal resonance model is based on the assumption that a temporary molecular negative-ion state (resonance) is formed and that this resonance accounts for the coupling of the electronic scattering dynamics with the nuclear motion (see [26] for a comprehensive review). The resonance is represented by a square-integrable discrete state $|\varphi_d\rangle$ which interacts with a continuum of scattering states $|\varphi_\varepsilon\rangle$ via coupling matrix elements $V_{d\varepsilon}$. Note that the discrete state $|\varphi_d\rangle$ is explicitly removed from the continuum using the projection operator formalism. The states $|\varphi_d\rangle$ and $|\varphi_\varepsilon\rangle$ are assumed to be diabatic states; that is, their wave functions should vary smoothly with internuclear distance $R$. Their derivatives with respect to $R$ can then be neglected in the spirit of the Born-Oppenheimer approximation. The essential ingredient of the nonlocal resonance model is the explicit consideration of threshold effects which enter through the threshold expansion of the energy-dependent width function

$$\Gamma(\varepsilon) = 2\pi|V_{d\varepsilon}|^2 \tag{4}$$

and the associated level shift $\Delta(\varepsilon)$ [26]. The behavior of the function $\Gamma(\varepsilon)$ close to origin is determined by long-range interaction potentials of the electron with the molecule. In the case of electron scattering from the $H_2$ in its $X^1\Sigma_g^+$ ground state, the negative-ion resonance is of $^2\Sigma_u$ symmetry and can decay by releasing electrons with odd angular momentum $l$. It is assumed that for low energies only $l=1$ is important. The threshold law of Wigner then yields

$$\Gamma(\varepsilon) \sim \varepsilon^{3/2} \tag{5}$$

for $\varepsilon \to 0$. There is another resonance of $^2\Sigma_g$ symmetry associated with the $H^-+H$ asymptote. However, its potential-energy function is repulsive and we neglect its influence on low-energy cross sections. The effect of this resonance on the scattering cross section has been studied within the local complex potential method in [20] and was found to be important only for electron energies $\varepsilon > 6$ eV.

The basic equation of the nonlocal resonance theory is the equation for nuclear motion in the short-lived anion state described by the projection of the full wave function of the system on the discrete state [26]:

$$|\Psi_d\rangle = \langle\varphi_d|\Psi\rangle\rangle. \tag{6}$$

With the double-ket $|\rangle\rangle$ notation we want to emphasize the fact that the full wave function contains both electronic and nuclear coordinates as dynamical variables, while the elec-

tronic coordinates are absent in the projected wave function $|\Psi_d\rangle$. The form of the equation of motion for $|\Psi_d\rangle$ depends on the boundary conditions which are different—for example, for electron-molecule scattering ($e+H_2$) and ion-atom scattering ($H^-+H$). In the case of the DA process, it is simpler to calculate the cross section from the wave function fulfilling the outgoing wave boundary condition for the $H^-$ +H channel. The equation of motion in its integral form then reads [26]

$$|\psi_j\rangle = |\phi_j\rangle + G_j(E)[V_d + F_j]|\psi_j\rangle, \tag{7}$$

where $|\psi_j\rangle$ is the $j$th component of the partial-wave expansion of the wave function $|\Psi_d\rangle$ and $V_d$ is the diabatic potential energy for the discrete state $|\varphi_d\rangle$. The wave function $|\phi_j\rangle$ and the Green's function $G_j(E)$ are known solutions for the free motion of the nuclei (see [39] for details). The action of the nonlocal energy-dependent potential $F_j$ in the coordinate representation is

$$F_j\psi_j(R) = \int dR' \int d\varepsilon V_{d\varepsilon}(R) g_j(E-\varepsilon, R, R') V^*_{d\varepsilon}(R')\psi_j(R'), \tag{8}$$

$g_j(E)$ being the partial-wave component of the Green's function for the adiabatic motion of nuclei in the ground-state potential $V_0(R)$ of neutral $H_2$. The non-Hermitian operator $F_j$ is the nonlocal energy-dependent effective potential which accounts for the decay of the discrete electronic state through the coupling with the electronic scattering continuum.

The cross section for DA of an electron of energy $\varepsilon_i$ to a molecule in the vibrational state $|\chi_j^v\rangle$ with the energy $E_j^v$ is given by [26]

$$\sigma_{DA}(\varepsilon_i) = \frac{4\pi^2\mu}{\varepsilon_i}|\langle\psi_j|V_{d\varepsilon_i}|\chi_j^v\rangle|^2. \tag{9}$$

Here the total energy $E$ equals the sum of the initial electron energy $\varepsilon_i$ and the energy of the initial molecular state $E_j^v$.

In the above description of the dynamics we neglected the coupling of the angular momentum $l=1$ of the electron with the angular momentum $j$ of the nuclear motion. The electronic and nuclear angular momenta are thus conserved. This is a good approximation as the consequence of the large mass difference of electrons and nuclei. In the previous work [39] we have included angular momentum recoil. We found only a small effect on the final integral DA cross sections which lies within the difference between the cross sections for angular momentum $j$ and $j\pm1$. Let us stress, however, that the $p$-wave character of the resonance is contained in the threshold behavior (5) of the discrete state-continuum coupling.

The nonlocal resonance model is characterized by the three functions $V_0(R)$, $V_d(R)$, and $V_{d\varepsilon}(R)$. The target potential-energy function $V_0(R)$ can directly be obtained from *ab initio* calculations. The functions $V_d(R)$ and $V_{d\varepsilon}(R)$ representing the $H_2^-$ resonance (at short internuclear distance) and the $H_2^-$ bound state (at intermediate and large internuclear distances) have been obtained using the projection operator formalism [25,41]. The potential function $V_d(R)$ for large $R$ [39] has been recovered from accurate *ab initio* calculations [40] of the $H_2^-$ potential energy function. All parameters of the model are thus determined by *ab initio* calculations. For convenience (and to correct some misprints in [25]) we provide a complete description of the model in the Appendix.

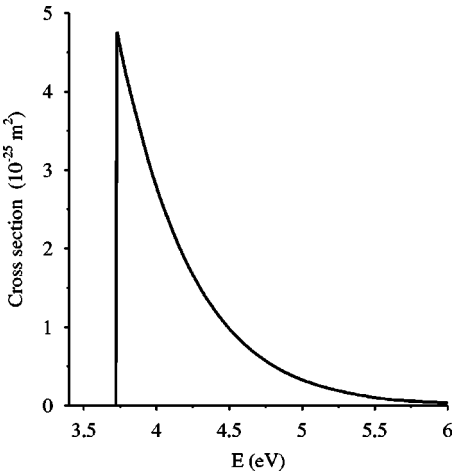


FIG. 1. Calculated dissociative attachment cross section for the target state $v=0$, $J=0$.

### B. Numerical methods

The nuclear wave function $\Psi_d(R)$ is represented by a partial-wave expansion with respect to rotational angular momentum. The Lippmann-Schwinger equation (7) is solved for the individual partial-wave components $\psi_j(R)$. For this purpose, the efficient Schwinger-Lanczos continued-fraction method [42] is employed. The Green's function $g_j$ in Eq. (8) is expanded in the basis of eigenstates of $V_0(R)$ including a discretized continuum. Typically much fewer than 100 states are needed to get converged results. A more detailed description of the numerical procedure is given in [39]; see also [38] for further developments of the method. The high efficiency of this method allows the cross sections to be calculated on a very fine mesh of collision energies for many channels.

## III. DISSOCIATIVE ATTACHMENT CROSS SECTIONS

### A. Target molecule in the ground rovibrational state

The calculated DA cross section for the ground rovibrational state of the hydrogen molecule is shown in Fig. 1. The DA cross section is rather small, reaching a peak value of about $5\times10^{-5}$ Å$^2$ at the threshold. The cross section has a near-perpendicular onset, followed by an exponential decrease.

### B. Role of vibrational excitation of the target

It is well known [21] that the magnitude of the DA cross section in the low-energy range increases rapidly with increasing vibrational quantum number of the target molecule; the magnitude of the DA cross section increases by nearly

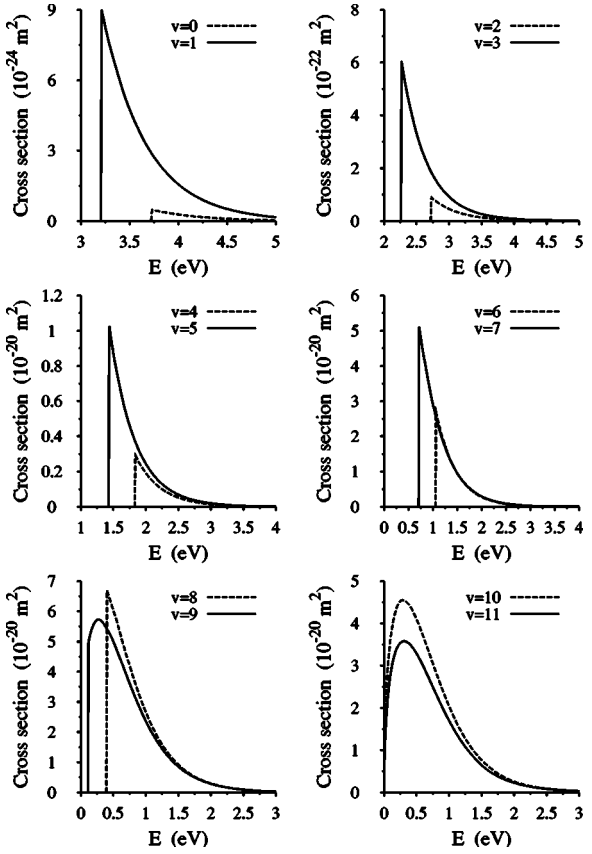


FIG. 2. Calculated DA cross section for a set of initial vibrational target states $v$. The rotational quantum number is $J=0$.

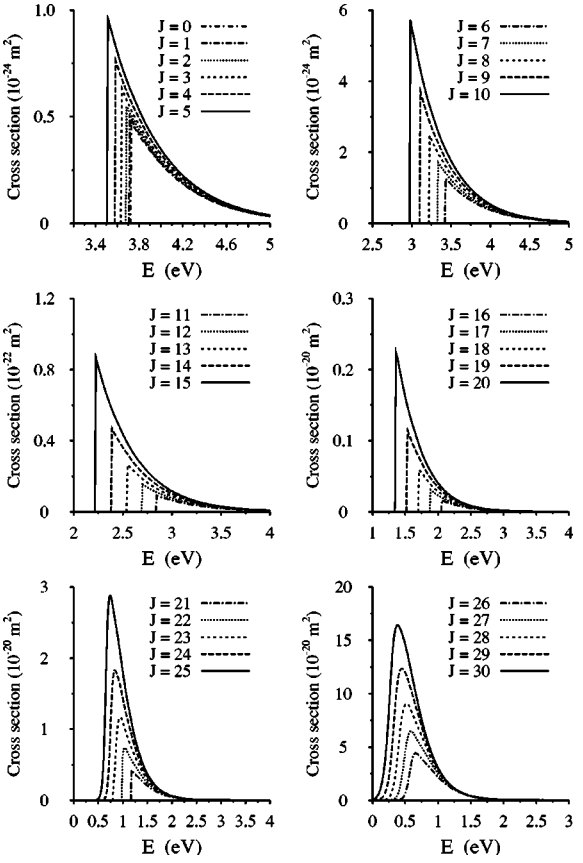


FIG. 3. Calculated DA cross sections for $v=0$ and $J=0,1,\ldots,30$.

five orders of magnitude from $v=0$ to $v=8-9$. This feature can be used, for example, as a diagnostic tool for the detection of vibrationally excited hydrogen [43–47] and also explains the high current of $H^-$ ions in $H^-$ production devices. This feature is illustrated in Fig. 2 where DA cross sections calculated by the present theory are plotted for a series of initial vibrational states, $v=0-11$.

### C. Role of the rotational excitation of the target

It is generally accepted that the effect of rotational excitation on the DA cross section $\sigma_{DA}$ is comparatively small and that the effect of vibrational excitation is responsible for the observed increase of $\sigma_{DA}$ with temperature; see, e.g., [48]. The effect of rotational excitation of the target as obtained by the present method is shown for $v=0$ in Fig. 3. As in the case of vibrational excitation, the DA cross section increases with increasing rotational quantum number $J$.

In Fig. 4 we analyze the relative sensitivity of the DA cross section on vibrational and rotational excitations by comparing several DA cross sections with nearly identical threshold energies. The DA cross section for the state $v=1$, $J=0$ is indeed much larger than the cross section for $v=0$, $J=8$. This is true only, however, at low values of the rotational quantum number $J$. With increasing $J$, the DA cross section changes its form; the onset becomes smooth and the cross sections attain their maxima at energies above the threshold. With increasing $J$, the rotational heating becomes more efficient than the vibrational heating. The largest DA cross section predicted by the present model arises for $v=1$, $J=29$ with a peak value of 28.3 Å$^2$ at $E=134$ meV. At this energy the DA process is exothermic; see Fig. 5. The highest cross section for an endothermic DA process is obtained for $v=2$, $J=23$. This reaction opens at 113 meV and the cross section reaches the value of 20.1 Å$^2$ at 249 meV. The maxima of DA cross sections for all $J$ are given in Table I. The third column in Table I denotes the energy at which the respective DA cross section attains its maximum.

### D. Comparison with experiment

The first measurement of the DA cross section of $H_2$ in the 4-eV region was carried out by Schulz and Assundi [10]. $H^-$ formation was observed with a very sharp onset at an electron energy $3.73\pm0.07$ eV. The measured cross section was found to be small, of the order of $10^{-5}$ Å$^2$. The magnitude of the 4-eV peak was measured relative to the height of the 14-eV peak. Schulz and Asundi found that the ratio of the magnitudes of the two peaks is approximatively 8%. Two absolute measurements of the 14-eV peak exist in the literature. A value of $3.5\times10^{-4}$ Å$^2$ has been measured by Schulz and Asundi [9], while a value $2.1\times10^{-4}$ Å$^2$ was obtained by Rapp *et al.* [11]. As a consequence of this uncertainty, two values of the peak cross section—namely, $2.8\times10^{-5}$ Å$^2$ and $1.6\times10^{-5}$ Å$^2$, exist in the literature. The measurement of

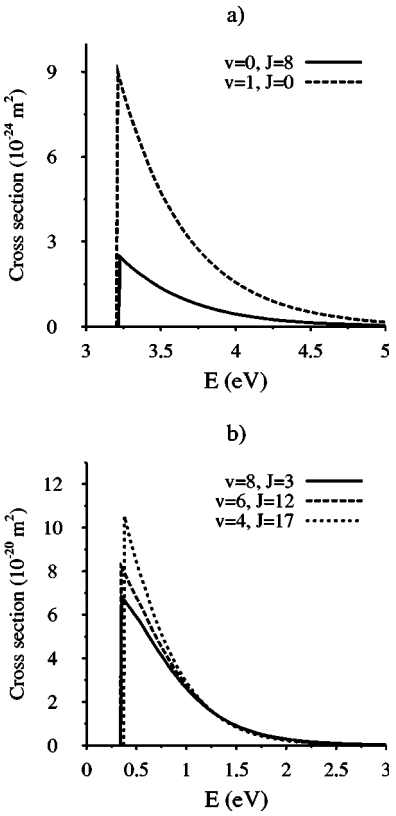


FIG. 4. DA cross sections for several excited target states with nearly identical threshold energies.

Schulz and Asundi was done at a temperature of about 300 K with an energy resolution of about 450 meV. If our cross section is evaluated at this temperature[1] and convoluted with the assumed experimental energy resolution, we obtain a value of $2.85\times10^{-5}$ Å$^2$, in full agreement with the measurement of Schulz and Asundi [10], provided we accept the larger experimental value; see Fig. 6.

It has been known for a long time that the shape of the measured DA cross section does not agree with the shape predicted by any of the proposed theories; all calculated DA peaks were broader than the measured peak. The shape of the DA cross section in the 4 eV region was recently remeasured by Drexel *et al.* [13]. They found that in the experiment of Schulz and Asundi the extraction field used to collect the emerging negative ions was too low to collect all of them. If a higher extraction field is applied, the DA peak gets broader, in full agreement with the calculations. This is demonstrated in Fig. 7, where we show different measurements normalized to the peak value of the theoretical cross section to reveal the differences in the cross-section shapes. (Here the experimental cross section denoted as Drexel1 was obtained with a low extraction field; the Drexel2 cross section corresponds to a higher extraction field. For details, see the original paper [13].) The theoretical cross section is calculated at the temperature $T=400$ K and convoluted with the energy resolution of 0.2 eV according to [13]. As it should be the calculated DA cross section agrees very well with Drexel1 in the low-energy region and with Drexel2 at higher energies.

[1]The cross section is calculated by averaging the individual DA cross sections of rovibrationally excited states over the Maxwell-Boltzmann distribution for a given temperature. Excited states do not contribute significantly for 300 K.

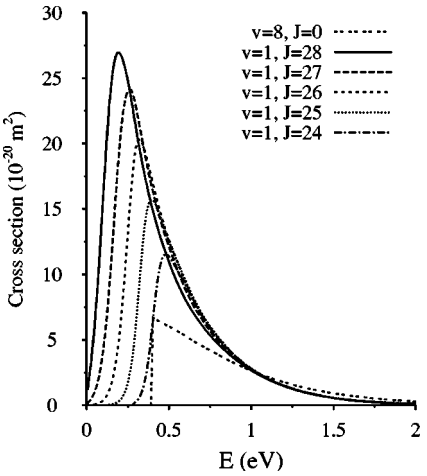


FIG. 5. DA cross sections for rotationally excited hydrogen molecules. The largest DA cross section is obtained for $v=1$ and high rotational states.

### E. Temperature effect

Experimentally, it is difficult to prepare the target molecule in a specific vibrationally excited state. However, a mixture of excited states with populations given by the Boltzmann distribution can be prepared by heating the target gas. The DA cross sections at higher temperatures were measured by Allan and Wong [14]. The measured (relative) cross sections are compared with the calculated ones in Fig. 8 for $H_2$ and in Fig. 9 for $D_2$. The experimental relative cross section are normalized to calculated absolute values at the peak value. An almost perfect agreement can be obtained by assuming a temperature which is higher than that specified by the experiment. The dashed line was obtained for the temperature of 1670 K in the case of $H_2$ and for 1550 K in the case of $D_2$. At higher energies (above about 3.8 eV) the calculated cross section is higher than the measured one even at the increased temperature. This may reflect the problem of low detection efficiency for higher ion energies discussed by Drexel *et al.* [13] and mentioned in the previous section. This may also explain the difference in the temperatures, since the measured cross sections for each excited state may be too narrow, thus lowering the summed cross section at the position of the main peak. We tried to compensate for such an affect including different detection efficiencies for $H^-$ with different energies into our calculation. We found that such a modification can slightly improve the disagreement in temperatures, but it cannot explain difference of several 100 K. Further experimental investigations would be highly desirable.

### F. Other theoretical data

Figure 10 gives a comparison of selected theoretical DA cross sections of $H_2$ in its ground rotational and vibrational

TABLE I. Maximum DA cross sections for individual states $(v,J)$. The threshold energies are given in the third column. In the fourth column the energy at which the cross section attains its maximum is given.

| $J$ | $v$ | $E_{thr}$ (eV) | $E_{max}$ (eV) | Cross section (Å$^2$) |
|---|---|---|---|---|
| 0 | 8 | 0.396 | 0.402 | 6.688 |
| 1 | 8 | 0.387 | 0.393 | 6.716 |
| 2 | 8 | 0.370 | 0.376 | 6.764 |
| 3 | 8 | 0.343 | 0.349 | 6.818 |
| 4 | 8 | 0.309 | 0.315 | 6.847 |
| 5 | 8 | 0.266 | 0.272 | 6.785 |
| 6 | 8 | 0.216 | 0.262 | 6.593 |
| 7 | 7 | 0.453 | 0.460 | 6.939 |
| 8 | 7 | 0.384 | 0.390 | 7.276 |
| 9 | 7 | 0.309 | 0.315 | 7.477 |
| 10 | 7 | 0.228 | 0.244 | 7.276 |
| 11 | 6 | 0.440 | 0.446 | 7.630 |
| 12 | 6 | 0.341 | 0.347 | 8.207 |
| 13 | 6 | 0.238 | 0.245 | 8.208 |
| 14 | 5 | 0.435 | 0.441 | 8.498 |
| 15 | 5 | 0.316 | 0.322 | 9.452 |
| 16 | 5 | 0.194 | 0.201 | 9.301 |
| 17 | 4 | 0.374 | 0.381 | 10.52 |
| 18 | 4 | 0.239 | 0.245 | 11.50 |
| 19 | 3 | 0.414 | 0.430 | 11.63 |
| 20 | 3 | 0.265 | 0.281 | 15.08 |
| 21 | 3 | 0.116 | 0.132 | 17.16 |
| 22 | 2 | 0.238 | 0.330 | 17.80 |
| 23 | 2 | 0.113 | 0.249 | 20.10 |
| 24 | 2 | 0.0 | 0.159 | 22.14 |
| 25 | 2 | 0.0 | 0.101 | 21.97 |
| 26 | 1 | 0.0 | 0.320 | 20.31 |
| 27 | 1 | 0.0 | 0.262 | 24.12 |
| 28 | 1 | 0.0 | 0.197 | 26.97 |
| 29 | 1 | 0.0 | 0.134 | 28.32 |
| 30 | 1 | 0.0 | 0.095 | 26.70 |

states. The calculated cross sections are denoted as follows: (a) present results, (b) Bardsley and Wadehra [19,20], (c) Fabrikant *et al.* [15], (d) Gauyacq [16], (e) Gertitschke and Domcke [28], and (f) Hickman [29]. The shape of all cross sections is very similar: a near-vertical onset followed by an exponential decrease. The peak values of the cross sections, however, differ significantly, ranging from $1.6\times10^{-5}$ Å$^2$ to $5\times10^{-5}$ Å$^2$. The largest value is obtained by the present *ab initio* calculation (solid line). Next to it is the DA cross section of the nonlocal resonance model of Gertitschke and Domcke [28]. Both calculations treat the process on the same level of theoretical description, but in the present model the long-range part of the $H+H^-$ potential at large and intermediate distances is more accurate. The long-range $H+H^-$ potential of the present model is more attractive than the interaction of the older model of Gertitschke and Domcke [28].

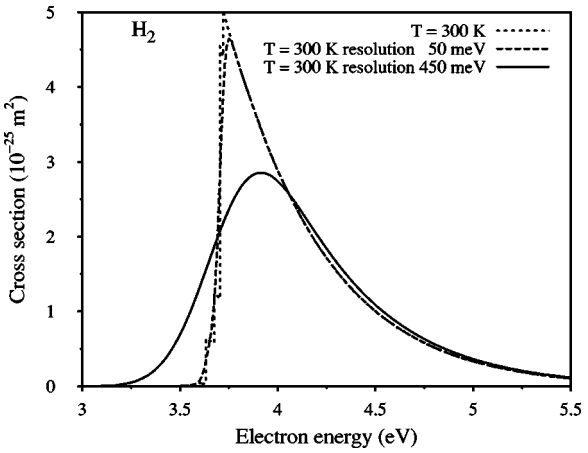


FIG. 6. DA cross section in $H_2$ calculated for the temperature $T=300$ K with three energy resolutions of the electron beam: $\Delta E=0$, 50, and 450 meV. In the experiment of Schulz and Asundi [10] the resolution was 450 meV.

This feature is reflected in the increase of the DA cross section near threshold. The calculation of Fabrikant *et al.* is based on a similar treatment of the nonlocal dynamics, but the parameters of the model are slightly different and the semiclassical approach [15,32] is used for the solution of the dynamical equation. The cross section of Gauyacq [16] has been obtained by a completely different approach. This theory is based on a zero-range model for the electron- $H_2$ interaction and a resonance is not explicitly introduced. The parameters of the zero-range model have been partly taken from *ab initio* calculations and partly fitted to reproduce the experimental cross section. The theory of Bardsley and Wadehra [19,20] uses the local approximation and the parameters are fitted to the experimental data. Finally, the calculation of Hickman [29] treats the nonlocal problem in the approximation of open channels. The nonlocal complex potential is determined from the *ab initio* data of [25]. This list of calculations is not complete; see, for example, [17,23,36].

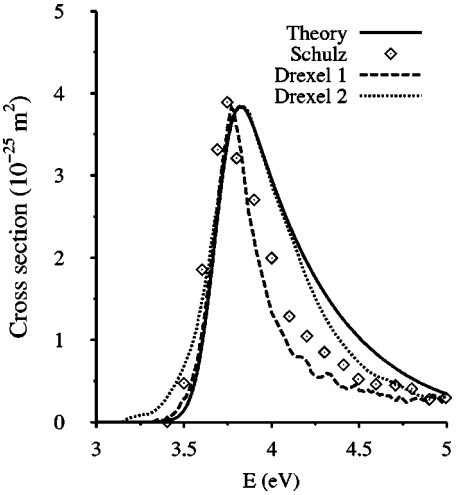


FIG. 7. Comparison of the shape of the DA cross section between the present theory and experiments of Schulz and Asundi [10] and Drexel *et al.* [13].

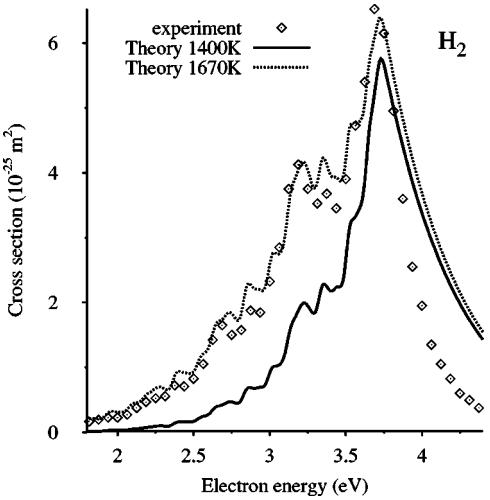


FIG. 8. Calculated DA cross section of $H_2$ for two temperatures, in comparison with the experimental data of Allan and Wong, for $T=1400$ K.

All the theories mentioned above predict an increase of the DA cross section with $v$, but the extent of the increase differs significantly from theory to theory. Usually, the dependence of the DA cross section on $v$ is plotted on a logarithmic scale, which blurs the differences among the different theories. To exhibit more clearly the differences among the existing calculations we plot in Fig. 11 the peak values of the DA cross sections calculated by various theories relative to the present results [i.e., $\sigma_{\mathrm{DA}}(v)/\sigma_{\mathrm{DA\ present}}(v)$] on a linear scale for a range of vibrational target states: (a) present result, (b) Hickman [29], (c) Fabrikant *et al.* [15], and (d) Bardsley and Wadehra [19,20]. The dependence of the DA cross section on $v$ differs very much from theory to theory. This behavior deserves further study.

In Fig. 12, the dependence of the peak value of the DA cross section on the rotational quantum number $J$ of the target obtained by various theories is plotted relative to the

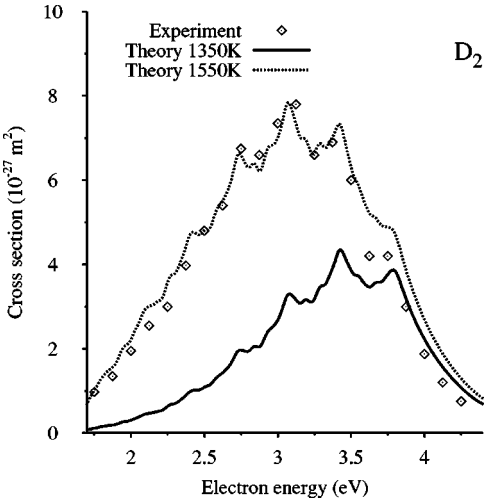


FIG. 9. Calculated DA cross section of $D_2$ for two temperatures, in comparison with experimental data of Allan and Wong, for $T=1350$ K.

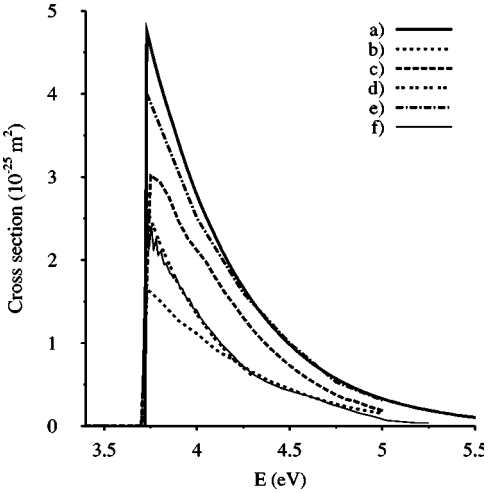


FIG. 10. Theoretical cross sections for DA to the ground target state $v=0$ and $J=0$. (a) Present results, (b) Bardsley and Wadehra [19,20], (c) Fabrikant *et al.* [15], (d) Gauyacq [16], (e) Gertitschke and Domcke [28], and (f) Hickman [29].

present results [i.e., $\sigma_{\mathrm{DA}}(J)/\sigma_{\mathrm{DA\ present}}(J)$]: (a) present results defined as unity, (b) Launay *et al.* [23], case V1, (c) Bardsley and Wadehra [19,20], and (d) Launay *et al.* [23], case V2. Again the trends differ, significantly from theory to theory. It is noteworthy that the other theories predict a less pronounced enhancement of the DA cross section with $J$ than the present calculation. Both nonlocal effects as well as differences in the long-range part of the $H_2^-$ potential-energy function in the earlier calculations may be responsible for this effect.

## IV. ORBITING RESONANCES IN DA

Resonance theories often use the local complex negative-ion potential for the interpretation of the results. The mathematical relation of this potential to model paraters $V_0$, $V_{\mathrm{d}}$, and $V_{\mathrm{d}\epsilon}$ has been discussed elsewhere [26,39]. The real part

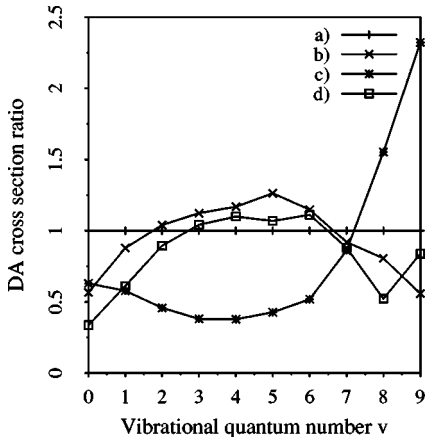


FIG. 11. Calculated peak values of DA cross sections plotted relative to the present result $[\sigma_{\mathrm{DA}}(v)/\sigma_{\mathrm{DA\ present}}(v)]$ for a set of vibrational states $v$. (a) Present result, (b) Hickman [29], (c) Fabrikant *et al.* [15], and (d) Bardsley and Wadehra [19,20].

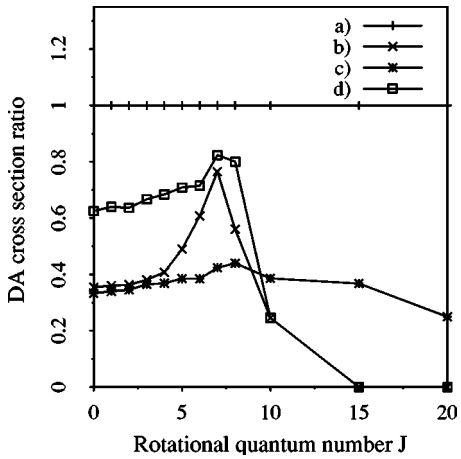


FIG. 12. The role of rotational excitation of the target on the peak DA cross sections plotted relative to the present results: (a) Present results, (b) Launay *et al.* [23], case V1, (c) Bardsley and Wadehra [19,20], and (d) Launay *et al.* [23], case V2.

$V_{\mathrm{res}}(R)$ of this potential corresponds to the energy of the negative-ion resonance state at short internuclear distances and to the energy of the bound state at large distances. The latter exhibits the polarization form $-C_4R^{-4}$ at large $R$. Contrary to the vibrational excitation of the target, which essentially only puts energy into the system, the rotational excitation changes the underlying interactions by adding the centrifugal term $J(J+1)/R^2$ to all radial potentials. Owing to this modification, all potential curves shift to higher energies with increasing $J$ and a barrier develops at intermediate internuclear distances. In Fig. 13, upper part, the potentials $V_0(R)$, $V_{\mathrm{d}}(R)$, and $V_{\mathrm{res}}(R)$ of the model are plotted for $J=0$. In the lower part of Fig. 13, the real part of the negative ion potential, $V_{res}(R)$, is plotted for three values of $J$, $J=22$, 23, 24. Two types of barriers are recognized: the centrifugal barrier at a distance of about 15 a.u. (only partly seen in this figure) and a short-range barrier at $R\sim 3$ a.u. For the particles to escape the autoionization region, the former barrier must be overcome. As a result one should expect that the DA cross section will be reduced near threshold for these values of $J$.

The role of the inner barrier is somewhat less clear. The barrier is located in the region of small $R$, where nonlocal forces are important and the local approximation is only of descriptive value. In fact, in our approach the resonance potential $V_{\mathrm{res}}(R)$ never enters the calculation. One may expect, however, that around $J\sim 23$ the DA cross section may change its shape at energies close to the threshold and irregularities in the $J$ dependence and energy dependence of the cross section may appear.

Figure 14 shows a detailed view of such an irregularity. A very sharp structure, with a width of about 1 meV, is observed here. At the threshold the cross section is very small. At an energy of about 20 meV above the threshold, the cross section rapidly increases, reaching a value of about 0.65 $\mathrm{Å}^2$, and then drops again. To interpret this structure, we plot in Fig. 14, lower part, the squared modulus of the nuclear wave functions at three energies around the peak energy. The wave functions are typical for an orbiting resonance. Note that the

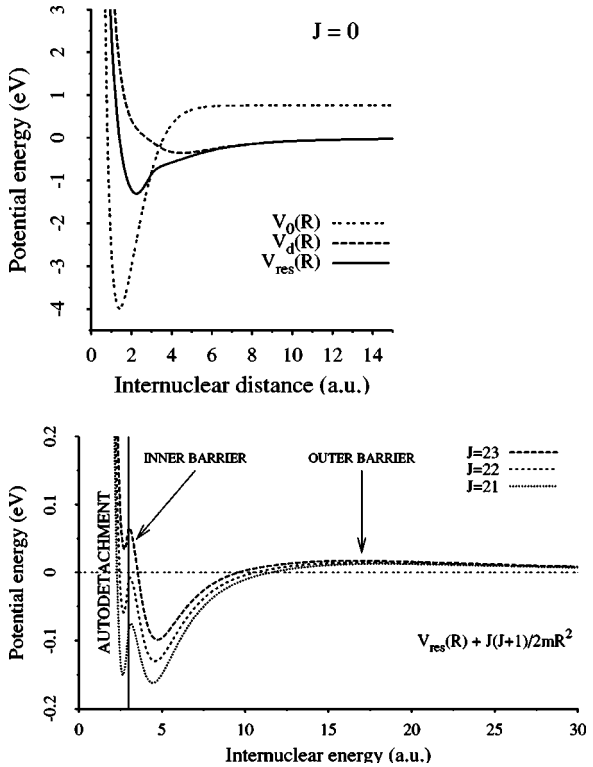


FIG. 13. Upper part: the potential-energy functions of the nonlocal resonance model for $J=0$: Solid line: resonance-state potential. Dashed line: discrete-state potential. Double-dashed line: molecular ground-state potential. Lower part: real part of the negative-ion potential for three values of $J$, $J=22$, 23, and 24. Two types of barriers are recognized as indicated. Outer radius of the autodetachment region is marked by the vertical line.

function is found from Eq. (7) with an outgoing boundary condition, which means that the normalization for large $R$ is prescribed. At energies outside the sharp peak, the magnitude of the inner part of the wave function is strongly suppressed. At the peak energy the wave function penetrates strongly into the inner part between the outer and inner barriers. At the peak energy the nuclear wave function is localized in the inner part of the interaction region in between the inner barrier and the outer (centrifugal) barrier. The resonance is thus the manifestation of tunneling enhancement due to the existence of quasibound states inside the double-barrier structure. The inner barrier prevents the broadening of the resonance due to fast decay through autodetachment in the region $R<3$ a.u. Observe that the wave function has four nodes between the barriers. This means that four other resonances with lower energies are to be expected. They are located below the DA threshold but can be observed in vibrational excitation cross sections and will be discussed briefly also in paper II. The quasibond states $H_2^-$ associated with the resonances have lifetimes many orders of magnitude higher than the natural lifetime of the $H_2^-$ collision complex. The properties of these unusual species will be discussed in a separate paper.

## V. ISOTOPE EFFECT IN DA

Another open problem in low-energy electron hydrogen scattering is the magnitude of the isotope effect. It is well

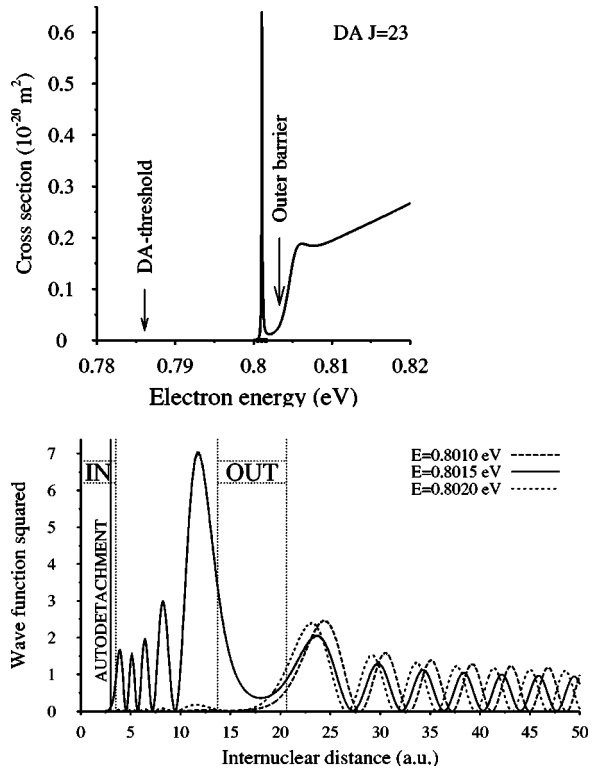


FIG. 14. Upper panel: detailed view of the DA cross section near threshold for $J=23$. The threshold energy and the top of outer centrifugal barrier are marked with arrows. Lower panel: the wave function squared for three energies around resonance at 0.8015 eV. The classically forbidden regions for inner and outer barriers are marked together with the autodetachment region. The energies at which the wave functions are calculated are also indicated by dots on the energy axis in the upper panel.

known that in the energy range considered in this paper, the DA cross section exhibits an extremely large dependence on the nuclear mass of the molecule. According to the measurement of Schulz and Assundi [10], the peak cross section is reduced by a factor of about 10 in HD relative to $H_2$ and the $D_2$ DA cross section is about 200 smaller than the $H_2$ DA cross section. This large isotope effect is explained by the extremely short autodetechment lifetime of the $^2\Sigma_u^+$ resonance which results in a strong decrease of the survival factor for $D_2$ relative to $H_2$. In Table II we summarize results for the isotope effect of some representative calculations in comparison with the experimental data.

It is seen that most calculations predict qualitatively correctly the pronounced isotope effect. Quantitatively, the results differ by a factor of more than 2 (excluding the early calculation [18]). The present model yields a value of about 300 for the ratio of the $H_2/D_2$ peak cross sections, whereas the earlier model of Mündel, Berman, and Domcke [25] predicted a value of about 200, in excellent agreement with the measurement. As explained above, these two models differ mainly in the long-range part of the $H+H^-$ interaction; this potential function is more attractive in the present model. The isotope effect is thus sensitive to the long-range part of the interaction.

To reveal the role of the rotational excitation, we present in Table III the DA cross sections for $H_2$, HD, and $D_2$ together with their ratio as a function of $J$. The ratio of the DA cross sections increases rapidly with $J$. This feature does not indicate, however, a rapid increase of the isotope effect with temperature, because the rapid increase is partly caused by the different shift of the DA thresholds to lower energy for $H_2$ and $D_2$ molecules. This problem was discussed some time ago by Christophorou [48]; see also [18].

TABLE II. Isotope effect in DA. Expt.: experimental data of Schulz and Asundi [12]. CP67: survival probability calculation of Chen and Peacher [18]. BW79: local calculation of Bardsley and Wadehra [20]. DP80: calculation of Drukarev and Pozdneev [49] based on the use of Faddeev equations. G85: calculation of Gauyacq [16]. MBD85: calculation of Mündel, Berman, and Domcke [25]. CHD98: calculation of Čížek, Horáček, and Domcke [39]. XF01: calculation of Xu and Fabrikant [35].

| | Expt. | CP67 | BW79 | DP80 | G85 | MBD85 | CHD98 | XF01 |
|---|---|---|---|---|---|---|---|---|
| $D_2$ | 1 | 1 | 1 | 1 | 1 | 1 | 1 | 1 |
| HD | 12 | 5.01 | - | 17 | - | - | 8.7 | 10 |
| $H_2$ | 200 | 55.9 | 533 | 200 | 430 | 200 | 300 | 402 |

It is important to stress that the DA cross section for $D_2$ is extremely small and very difficult to measure precisely. Moreover, this cross section was measured only once a long time ago. A new measurement of the DA cross section of $D_2$ is highly desirable.

The present value of the isotope effect shown in Table II was obtained for $v=0$ and $J=0$. In a real experiment carried out at a finite temperature, higher rotational states are involved. In order to render our comparison with experiment more reliable, we calculated the DA cross section assuming a target temperature of $T=300$ K as in the experiment of Schulz and Asundi. Moreover, it has been shown above that the finite energy resolution of the electron beam reduces the DA cross section. This is shown in Fig. 6 for $H_2$ and in Fig. 15, upper part, for $D_2$. In the lower part of Fig. 15 the cal-

TABLE III. Isotope effect for the ground vibrational state $v=0$. DA $H_2$: DA cross section for $H_2$. DA HD: DA cross section for HD. DA $D_2$: DA cross section for $D_2$. Last column: ratio of DA cross sections for $H_2$ and $D_2$.

| $J$ | DA $H_2$ | DA HD | DA $D_2$ | DA $H_2/D_2$ |
|---|---|---|---|---|
| 0 | 4.86(−5) | 5.61(−6) | 1.60(−7) | 304 |
| 1 | 5.05(−5) | 5.86(−6) | 1.61(−7) | 314 |
| 2 | 5.56(−5) | 6.33(−6) | 1.74(−7) | 320 |
| 3 | 6.36(−5) | 7.19(−6) | 1.91(−7) | 333 |
| 4 | 7.72(−5) | 8.47(−6) | 2.18(−7) | 354 |
| 5 | 9.69(−5) | 1.03(−5) | 2.59(−7) | 374 |
| 6 | 1.26(−4) | 1.32(−5) | 3.12(−7) | 404 |
| 7 | 1.74(−4) | 1.76(−5) | 3.90(−7) | 446 |
| 8 | 2.51(−4) | 2.40(−5) | 5.05(−7) | 497 |
| 9 | 3.71(−4) | 3.37(−5) | 6.66(−7) | 557 |
| 10 | 5.74(−4) | 4.95(−5) | 9.17(−7) | 626 |
| 15 | 8.61(−3) | 5.47(−4) | 6.56(−6) | 1294 |

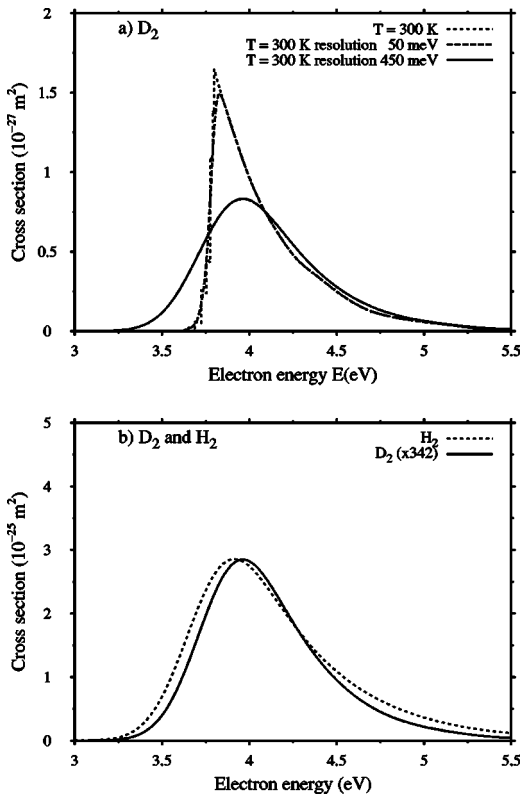


FIG. 15. DA cross section in $D_2$ calculated for the temperature $T=300$ K with three energy resolutions of the electron beam: $\Delta E=0$, 50, and 450 meV. (b) DA cross sections of $H_2$ (dashed line) and $D_2$, scaled up by a factor of 342 (solid line), for a target temperature of 300 K and an energy resolution of the electron beam of 450 meV.

culated DA cross section for $H_2$ is shown together with the DA cross section for $D_2$, multiplied by 342 to have equal peak values. Some differences are immediately observable. The $H_2$ DA cross section peaks at an energy $E=3.91$ eV and that for $D_2$ at a slightly higher energy $E=3.96$ eV, reaching the value $8.33\times10^{-8}$ Å$^2$. The $D_2$ peak is narrower than the $H_2$ peak by 90 meV full width at half maximum (FWHM). Hence, the ratio of $H_2/D_2$ cross sections depends on the energy resolution $\Delta E$ of the electron beam. This is demonstrated in Table IV.

## VI. SUMMARY AND CONCLUSIONS

An exhaustive computational investigation of the low-energy DA process in $H_2$ and its isotopomers has been performed within the framework of the nonlocal resonance theory. The calculations are based on the model developed by Čížek, Horáček, and Domcke [39] on the basis of *ab initio* fixed-nuclei electron-molecule scattering data [41] and an accurate calculation of the bound part of the $H_2^-$ potential energy function [40]. The efficient Schwinger-Lanczos continued-fraction method [42] has been employed for the solution of the nuclear dynamical problem. The computational efficiency of this method has allowed us to obtain DA cross sections for a large number of vibrational and rotational channels on a very fine energy grid. The latter aspect has been essential for the discovery of unexpected sharp spikes in the DA cross section due to long-lived $H+H^-$ orbiting resonances.

TABLE IV. Isotope effect as function of the energy resolution $\Delta E$ of the electron for a target temperature $T=300$ K.

| $T=300$ K | DA ratio | | |
|---|---|---|---|
| $\Delta E$ (meV) | 0 | 50 | 450 |
| $H_2/D_2$ | 305 | 311 | 342 |
| $H_2$/HD | 8.6 | 8.7 | 9.0 |

It has been shown that the theory reproduces the collision-energy dependence of the DA cross section in $H_2$ within the accuracy of the measurements [10,13]. More accurate measurements of the shape of the DA cross section with improved electron energy resolution and improved detection efficiency of $H^-$ are required to reveal possible limitations of the theory. The calculations support the larger of two reported values for the peak cross section in $H_2$ at $T=300$ K ($2.8\times10^{-21}$cm$^2$). More accurate measurements of the $H_2/D_2$ isotope effect also are desirable to confirm or refute the theoretically predicted value of 342 for the $\sigma_{DA}(H_2)/\sigma_{DA}(D_2)$ cross section ratio at $T=300$ K.

The calculations confirm the expected strong increase of $\sigma_{DA}$ with increasing vibrational excitation of the target gas. It has been shown that there is qualitative, but not quantitative, agreement between the existing calculations in this respect. The present calculations predict a considerably larger effect of rotational excitation on the DA cross section than has been found in previous calculations which invoked the local complex potential approximation [19,20]. The largest DA cross section, $28.3\times10^{-16}$ cm$^2$, is obtained for $v=1$, $J=29$. Rotational excitation thus contributes essentially to the enhancement of the DA process at elevated temperatures. The calculated DA cross sections of $H_2$ and $D_2$ at $T=1400$ K and $T=1350$ K, respectively, agree qualitatively with the measurements of Allan and Wong [14], but quantitative deviations exist.

As a new phenomenon, the existence of an unusual inner barrier in addition to the usual centrifugal barrier has been predicted for the radial potential energy function of the $^2\Sigma_u^+$ resonance [39]. This barrier suppresses the decay via autodetachment at short internuclear distances for certain values of $J(J\approx23$ in $H_2)$. As a result, a long-lived $H+H^-$ orbiting resonance exists and is reflected in a narrow spike in the DA cross section near threshold.

The nonlocal resonance model predicts, in addition to the DA cross section, also the cross sections for vibrational excitation and the cross section for associative detachment as well as the energy spectrum of the electrons resulting from the associative detachment process. The latter data have been discussed in detail in [39]. The results of a comprehensive investigation of the vibrational excitation cross sections of $H_2$ and its isotopomers are described in the accompanying paper II.

**ACKNOWLEDGMENTS**

We thank M. Allan, L. Pichl, and T. Kato for discussions. Support from Grants No. KONTAKT ME-562 MŠMT and No. GACR 202/02/D112 is acknowledged.

## APPENDIX: NONLOCAL RESONANCE MODEL FOR THE $^2\Sigma_u^+$ RESONANCE OF $H_2^-$

The construction of the model functions is described in [39]. We considered it useful to include detailed description of the model parameters here, since they were published partly in [39] and partly in [25] (with some misprints in the tables). Definition of the quantities $V_{d\varepsilon}(R)$ and $V_d(R)$ in terms of full electronic Hamiltonian $H_{el}$ of the system with internuclear distance $R$ fixed is given below, together with analytic fit of the $R$ and $\varepsilon$ dependences obtained from *ab initio* data.

The original model of Mündel, Berman, and Domcke (MBD) [25] was constructed from their "fixed- $R$ " *ab initio* electron-molecule scattering calculations. The function $V_0(R)$ in the MBD model is constructed as the spline interpolation of the data of Kołos and Wolniewicz [50]. The coupling of the discrete state of $^2\Sigma_u^+$ symmetry to the $p$-wave continuum was fitted with the formula

$$V_{d\varepsilon}(R) \equiv \langle \varphi_d | H_{el} | \varphi_\varepsilon \rangle = \frac{1}{\sqrt{2\pi}} \sum_{i=1}^{3} f_i(\varepsilon) g_i(R), \qquad \text{(A1)}$$

where

$$f_i(\varepsilon) = A_i \varepsilon^{\alpha/2} e^{B_i \varepsilon}, \quad i = 1,2,3,$$

$$g_i(R) = \exp[-C_i^2 (R - R_0)^2], \quad i = 1,2,$$

$$g_3(R) = \exp[-C_3 (R - R_0)].$$

The values of the constants are as follows (all quantities are in atomic units):

$$A_1 = 1.6618, \quad A_2 = 1.3603, \quad A_3 = 1.0467,$$

$$B_1 = 18.863, \quad B_2 = 4.6559, \quad B_3 = 1.4504,$$

$$C_1 = 0.2, \quad C_2 = 0.3302, \quad C_3 = 0.489,$$

$$\alpha = 1.5.$$

The equilibrium distance $R_0$ of $H_2$ is $R_0 = 1.4014$ a.u. [50].

In [39] we have replaced the original discrete state potential $V_d(R)$ with a new function to describe more accurately the behavior of the $H_2^-$ bound-state energy for larger internuclear separation $R$. The resulting potential function is

$$V_d(R) \equiv \langle \varphi_d | H_{el} | \varphi_d \rangle = \begin{cases} 1.74 e^{-2.37R} - \dfrac{94.4 e^{-22.5/R}}{[(R-2.54)^2 + 3.11]^2} & \text{for } R \leqslant 10.6, \\ -0.00845 R e^{-0.35R} - \dfrac{2.25}{R^4} - \dfrac{97}{R^6} & \text{for } R > 10.6. \end{cases} \qquad \text{(A2)}$$

[1] S. Lepp, P. C. Stancil, and A. Dalgarno, J. Phys. B **35**, R57 (2002).
[2] D. E. Post, J. Nucl. Mater. **220–222**, 143 (1995); S. I. Krasheninnikov, A. Yu Pigarov, and D. J. Sigmar, Phys. Lett. A **214**, 285 (1996).
[3] N. Ohno, N. Ezumi, S. Takamura, S. I. Krasheninnikov, and A. Yu. Pigarov, Phys. Rev. Lett. **81**, 818 (1998).
[4] J. R. Hiskes, Comments At. Mol. Phys. **19**, 75 (1987).
[5] J. R. Hiskes and A. M. Karo, Appl. Phys. Lett. **54**, 508 (1989).
[6] D. A. Skinner, A. M. Bruneteau, P. Berlemont, C. Courteille, R. Leroy, and M. Bacal, Phys. Rev. E **48**, 2122 (1993).
[7] R. H. M. Smit, Y. Noat, C. Untiedt, N. D. Lang, M. C. van Hemert, and J. M. van Ruitenbeek, Nature (London) **419**, 906 (2002).
[8] V. I. Khvostenko and V. M. Dukelskii, J. Exp. Theor. Phys. **34**, 1026 (1958); V. I. Khvostenko and V. M. Dukelskii, Sov. Phys. JETP **6**, 657 (1958).
[9] G. J. Schulz, Phys. Rev. **113**, 816 (1959).
[10] G. J. Schulz and R. K. Asundi, Phys. Rev. Lett. **15**, 946 (1965).
[11] D. Rapp, T. E. Sharp, and D. D. Briglia, Phys. Rev. Lett. **14**, 533 (1965).
[12] G. J. Schultz and R. K. Asundi, Phys. Rev. **158**, 25 (1967).
[13] H. Drexel, G. Senn, T. Fiegele, P. Scheier, A. Stamatovic, N. J. Mason, and T. D. Märk, J. Phys. B **34**, 1415 (2001).
[14] M. Allan and S. F. Wong, Phys. Rev. Lett. **41**, 1791 (1978).
[15] I. I. Fabrikant, J. M. Wadehra, and Y. Xu, Phys. Scr. **T96**, 45 (2002).
[16] J. P. Gauyacq, J. Phys. B **18**, 1859 (1985).
[17] F. Robicheaux, Phys. Rev. A **43**, 5946 (1991).
[18] J. C. Y. Chen and J. L. Peacher, Phys. Rev. **163**, 103 (1967).
[19] J. M. Wadehra and J. N. Bardsley, Phys. Rev. Lett. **41**, 1795 (1978).
[20] J. N. Bardsley and J. M. Wadehra, Phys. Rev. A **20**, 1398 (1979).
[21] J. M. Wadehra, Appl. Phys. Lett. **35**, 917 (1979).
[22] J. M. Wadehra, Phys. Rev. A **29**, 106 (1984).
[23] J. M. Launay, M. Le Dorneuf, and C. J. Zeippen, Astron. Astrophys. **252**, 842 (1991).
[24] R. Celiberto, R. K. Janev, A. Laricchiuta, M. Capitelli, J. M.

Wadehra, and D. E. Atems, At. Data Nucl. Data Tables **77**, 161 (1999).
[25] C. Mündel, M. Berman, and W. Domcke, Phys. Rev. A **32**, 181 (1985).
[26] W. Domcke, Phys. Rep. **208**, 97 (1991).
[27] P. L. Gertitschke and W. Domcke, J. Phys. B **24**, 367 (1991).
[28] P. L. Gertitschke and W. Domcke, Phys. Rev. A **47**, 1031 (1993).
[29] A. P. Hickman, Phys. Rev. A **43**, 3495 (1991).
[30] D. E. Atems and J. M. Wadehra, Phys. Rev. A **42**, 5201 (1990).
[31] D. E. Atems and J. M. Wadehra, J. Phys. B **26**, L759 (1993).
[32] G. A. Gallup, Y. Xu, and I. I. Fabrikant, Phys. Rev. A **57**, 2596 (1998).
[33] Y. Xu, A. K. Kazansky, and I. I. Fabrikant, Phys. Rev. A **63**, 014703 (2000).
[34] Y. Xu, G. A. Gallup, and I. I. Fabrikant, Phys. Rev. A **61**, 052705 (2000).
[35] Y. Xu and I. I. Fabrikant, Appl. Phys. Lett. **78**, 2598 (2001).
[36] A. K. Kazanskii, Opt. Spektrosk. **80**, 888 (1996).
[37] J. Horáček, M. Čížek, and W. Domcke, Theor. Chem. Acc. **100**, 31 (1998).
[38] P. Kolorenč, M. Čížek, J. Horáček, G. Milnikov, and H. Nakamura, Phys. Scr. **65**, 328 (2002).
[39] M. Čížek, J. Horáček, and W. Domcke, J. Phys. B **31**, 2571 (1998).
[40] J. Senekowitsch, P. Rosmus, W. Domcke, and H.-J. Werner, Chem. Phys. Lett. **111**, 211 (1984).
[41] M. Berman, C. Mündel, and W. Domcke, Phys. Rev. A **31**, 641 (1985).
[42] H.-D. Meyer, J. Horáček, and L. S. Cederbaum, Phys. Rev. A **43**, 3587 (1991).
[43] R. I. Hall, I. Čadež, M. Landau, F. Pichou, and C. Schermann, Phys. Rev. Lett. **60**, 337 (1988).
[44] I. Čadež, R. I. Hall, M. Landau, F. Pichou, and C. Schermann, J. Phys. B **21**, 3271 (1988).
[45] D. Popovič, I. Čadež, M. Landau, F. Pichout, C. Schermann, and R. I. Hall, Meas. Sci. Technol. **1**, 1041 (1990).
[46] S. Gough, C. Schermann, F. Pichou, M. Landau, I. Čadež, and R. I. Hall, Astron. Astrophys. **305**, 687 (1996).
[47] I. Čadež, R. I. Hall, M. Landau, F. Pichou, and C. Schermann, J. Chem. Phys. **106**, 4745 (1997).
[48] L. G. Christophorou, J. Chem. Phys. **83**, 6219 (1985).
[49] G. Drukarev and S. Pozdneev, J. Phys. B **13**, 2611 (1980).
[50] W. Kolos and L. Wolniewicz, J. Chem. Phys. **43**, 2429 (1965).